AGU100 ADVANCING EARTH AND SPACE SCIENCE

Geophysical Research Letters

RESEARCH LETTER
10.1029/2018GL079872

Key Points:
- Synthetic waveforms are shown to detect real earthquakes in matched-filter routines
- LFEs, aftershocks, and other seismicity can be detected with little a priori knowledge
- Matched-filters with synthetic templates outperform energy-based detection routines in some cases

Supporting Information:
- Supporting Information S1

Correspondence to:
C. J. Chamberlain,
calum.chamberlain@vuw.ac.nz

Citation:
Chamberlain, C. J., & Townend, J. (2018). Detecting real earthquakes using artificial earthquakes: On the use of synthetic waveforms in matched-filter earthquake detection. *Geophysical Research Letters*, *45*, 11,641–11,649. https://doi.org/10.1029/2018GL079872

Received 5 AUG 2018
Accepted 23 OCT 2018
Accepted article online 29 OCT 2018
Published online 9 NOV 2018

Detecting Real Earthquakes Using Artificial Earthquakes: On the Use of Synthetic Waveforms in Matched-Filter Earthquake Detection

C. J. Chamberlain[1] **and J. Townend**[1]

[1]School of Geography, Environment and Earth Sciences, Victoria University of Wellington, Wellington, New Zealand

Abstract Matched-filters are an increasingly popular tool for earthquake detection, but their reliance on a priori knowledge of the targets of interest limits their application to regions with previously documented seismicity. We explore an extension to the matched-filter method to detect earthquakes and low-frequency earthquakes on local to regional scales. We show that it is possible to increase the number of detections compared with standard energy-based methods, with low false-detection rates, using suites of synthetic waveforms as templates. We apply this to a microearthquake swarm and an aftershock sequence, and to detect low-frequency earthquakes. We also explore the sensitivity of detections to the synthetic source's location and focal mechanism. Source-receiver geometry has a first-order control on how sensitive matched-filter detectors are to variations in source location and focal mechanism, and this likely applies to detections made using both synthetic and real templates.

Plain Language Summary Matched-filters measure the similarity between continuous waveforms and template waveforms. These filters provide an effective means of detecting scaled copies of the template in seismic data, often enabling the detection of small earthquakes in noisy data. This makes them an excellent tool for detecting earthquakes in noisy environments or during sequences of many earthquakes occurring in a short time. However, matched-filters require a known waveform to look for and are therefore not useful when studying a new area with no prior information. This paper describes an extension to the matched-filter method in which synthetic waveforms are used as template events. We show that even simple synthetics generated using a very naïve model of the Earth and the earthquake source are capable of detecting real seismicity.

1. Introduction

Matched-filters are capable of detecting earthquakes under low-signal-to-noise ratio (SNR) conditions and within the coda of other earthquakes (e.g., Gibbons & Ringdal, 2006; Slinkard et al., 2013). Because of these advantages over standard energy-based detection routines, they have been successfully used to construct more complete aftershock catalogs (e.g., Kato & Obara, 2014; Peng & Zhao, 2009; Warren-Smith, Chamberlain, et al., 2017; Warren-Smith et al., 2018) and catalogs of swarm activity (e.g., Shelly, Hill, et al., 2013; Shelly, Moran, & Thelen 2013), as well as to provide observations of more esoteric signals such as low-frequency earthquakes (LFEs; e.g., Baratin et al., 2018; Frank et al., 2013; Shelly et al., 2007, 2009) and repeating earthquakes (e.g., Kato et al., 2012). However, matched-filters are only able to detect seismicity of similar location and focal mechanism to a previously known source. This reliance on a priori information precludes the application of matched-filters to the general earthquake detection problem.

We show that by using synthetic seismograms matched-filters can be used to detect earthquakes with limited a priori knowledge of the source. This is motivated by a need to generate accurate aftershock and swarm catalogs during the early phases of sequences in regions which previously had limited seismicity, and to detect weak signals, such as those produced by LFEs. Previous work by Rodgers et al. (2006) showed that synthetic waveforms could be used in subspace detection routines for nuclear explosions at teleseismic distances and at low frequencies (0–0.2 Hz) using seismic arrays. Ohta and Ide (2017) used stacked LFE waveforms and adjusted their moveouts to generate synthetic LFE templates for use in matched-filters. Here we show that on a local to regional scale with no real waveform information, we are able to use synthetics to detect real seismicity.

We outline two methods for generating synthetic templates and provide examples of their use. The resulting catalogs are compared with previously published catalogs and matched-filter-derived catalogs using real events as templates. Finally, we analyze the sensitivity of detections to source location and focal mechanism.

2. Methods

2.1. Synthetic Template Design

We conducted initial trials using simple synthetic templates composed of spikes convolved with decaying sine waves to represent *P* and *S* arrivals. These synthetics represent a naïve model of seismic waveforms with a simplistic theoretical basis but prove to be effective at detecting earthquakes in some cases. In the following we refer to synthetics generated this way as *naïve synthetics*. We subsequently experimented with synthetic templates generated using synthetic Green's functions computed using the *axitra* package (Coutant, 1989; https://isterre.fr/IMG/tgz/axitra.tgz, last accessed on: 8 December 2017); we refer to synthetics generated in this way as *Green's function synthetics*. Both forms of synthetic represent (to a greater or lesser extent) idealized waveforms corresponding to a specific hypocenter and focal mechanism.

2.1.1. Naïve Synthetics

We generate naïve synthetics by convolving a decaying sine wave with a time-series containing a spike representing the *P* arrival, and a series of spikes of decaying amplitude and alternating polarity representing the S-arrival (see Supplementary Information for more details). We use a sequence of spikes to represent the *S* arrival to simulate scattered arrivals in the coda of the *S* wave, with little regard for whether this is physically realistic. We advocate the use of multistation templates for these naïve synthetics to provide greater constraints on earthquake source location. We generate a series of single-channel naïve synthetics, each with their own calculated S−P time, and combine these by applying moveouts to the synthetic traces for each station appropriate for the modeled location. These synthetics have little physical basis other than arrival time information but do provide useful detections of real earthquakes in certain situations (see section 3). Because these synthetics require little computational effort to generate, many different synthetic templates can be generated and tested in a short time.

2.1.2. Green's Function Synthetics

We use the *axitra* code (Coutant, 1989) to generate synthetic Green's functions using 1-D velocity models. This code yields synthetics that match data reasonably well at frequencies above 1 Hz. Codes that accomodate 3-D velocity models may be more appropriate for distant sources, but for the local scales we considered here, the 1-D approach is sufficient. We generate Green's functions at 10 Hz and convolve them with a Ricker wavelet. The resulting seismograms are convolved with the relevant instrument response to generate final simulated waveforms, which is faster than removing the response from continuous data for small template sets.

2.2. Detection

Templates are correlated with continuous seismic data using the *EQcorrscan* package (Chamberlain et al., 2017). Data are filtered using a fourth-order Butterworth bandpass filter and resampled in the frequency domain. Normalized single-channel cross correlations are computed in the frequency domain, delayed according to the relative moveout of the template channel, and stacked to create a vector of cross-correlation sums. Detections are made when this cross-correlation sum exceeds a threshold based on the median absolute deviation (MAD) of the cross-correlation sum (Shelly et al., 2007). We vary the MAD multiplier for different examples to improve the quality of the detections.

3. Examples

In the following section we demonstrate that, with known phase arrivals, synthetic templates can be generated that match known waveforms sufficiently for detection. We then extend this by generating templates for a grid of unknown LFE sources. Finally, we test the sensitivity of detections to variations in source location and focal mechanism.

3.1. Swarm

Swarms are characterized by high rates of seismicity, which makes them difficult to study using energy-based detectors (Hainzl, 2016). In contrast, due to the high waveform similarities often observed in swarms, matched-filters work well in these situation (Shelly et al., 2013). We analyze a swarm in the central Southern Alps (New Zealand) previously studied by Boese et al. (2014). We use data recorded on the SAMBA (Boese et al., 2012) and GeoNet (Petersen et al., 2011) networks on 24 May 2009. We generate three sets of templates

from real waveforms, naïve synthetics, and Green's function synthetics. To generate the naïve synthetics, we use previously picked phase arrivals (Boese et al., 2014) to set the timing of the *P* and *S* arrivals. For the naïve synthetics we only synthesize data for stations with both *P* and *S* picks; we found that using synthetic *S* arrivals for stations with only *P* picks gave poor matches to the data with the simple 1-D velocity model available resulting in fewer detections.

To generate the Green's function synthetics, we use the 1-D velocity model that Boese et al. (2014) used to locate the events originally, and the density, Q_P, and Q_S values that Ristau (2008) used for South Island. Green's functions are generated for each template event and each station picked, using a representative focal mechanism for the swarm (282/84/145, strike/dip/rake in degrees from; Boese et al., 2014). Real templates are generated from the continuous waveform data. All templates are resampled to 25 Hz, bandpass filtered between 2 and 10 Hz, and cut to 6s length beginning 0.5 s before the pick-time (for *P* on the vertical channel and S on horizontal channels). We chose 6-s long templates to capture converted arrivals at distant stations in both the real and Green's function templates. Because the naïve synthetics do not include converted phases, we use 6-s windows beginning at the *P* arrival on both horizontal and vertical channels.

Prior to detection, we remove any template with waveforms from fewer than five stations. This leaves four naïve synthetic templates and 11 templates for both the real and Green's function synthetic template sets of a possible 17. Thirteen naïve synthetic templates are removed due to the restriction of only using stations with both *P* and *S* picks, and requiring at least five stations. In testing we found that allowing templates with fewer stations resulted in increased false-detection rates.

Finally, all template sets are correlated with 1 day of continuous data. Detections are made when the cross-correlation sum exceeds 8 × MAD. We remove detections within 2 s of another detection with a higher correlation sum to avoid duplicate detections. Finally, we remove any detections with a SNR below 3.0 to allow construction of second-generation templates from the detections: low SNR detections make poor templates. All template sets detect events from the swarm and, in the case of the Green's function synthetics and the real template sets, outperform the previous analysis by Boese et al. (2014) who made 17 detections (Figure 1). We make 41, 29, and 18, detections, for the real, Green's function synthetics and naïve synthetics sets, respectively. We make one false detection using the naïve synthetics and none for either the real or Green's function synthetic template sets. Using the waveforms of the detections as templates in a second iteration of detection yields 106, 141, and 83 detections for the real, Green's function, and naïve sets. An optimized energy detector (sta/lta) made 27 detections in the same period (see supporting information Figure S17).

3.2. Wanaka Aftershocks

Standard earthquake detection methods struggle to detect earthquakes within the early parts of aftershock sequences (Hainzl, 2016), which can adversely affect subsequent forecasts based on these incomplete catalogs (Gerstenberger et al., 2005). To demonstrate the ability of synthetics to detect in this period, we apply synthetic templates to the first day of the Wanaka *M*6.0 aftershock sequence (4 May 2015) previously analyzed by Warren-Smith, Chamberlain, et al. (2017).

This example uses data from the COSA ((Warren-Smith, Lamb, et al., 2017) and GeoNet (Petersen et al., 2011) networks, and the manual picks and initial locations generated by Warren-Smith, Chamberlain, et al. (2017) for 31 events recorded on the first day of the sequence. We use the same process to generate templates as described in section 3.1, except that we adopt the velocity model used by Warren-Smith, Chamberlain, et al. (2017) and the mainshock focal mechanism (252/58/170, strike/dip/rake in degrees) to synthesize Green's functions. After removing templates with fewer than five stations, we have 31 real and Green's function synthetic templates, and 26 naïve synthetic templates.

We correlate templates with 1 day of continuous waveform data and detect when the cross-correlation sum exceeds 9 × MAD (Warren-Smith, Chamberlain, et al., 2017 used a threshold of 10×MAD, but a denser template database; a higher threshold than that used for the swarm is required, because the assumption of randomly distributed correlation sums is violated). This results in 1,678, 248, 358 detections for the real, Green's function synthetics, and naïve synthetics template sets, respectively. We plot only the detections for the hour around the mainshock in Figure 2 for clarity. Visual inspection of the detections reveals that each template set makes two false detections in the 24-hr period (no visible earthquake arrivals). Note that in this example we do not remove low SNR detections because all had sufficiently high SNR to use as templates. Using the waveforms from these templates for a second round of detection results in 3,701 and 4,129 detections

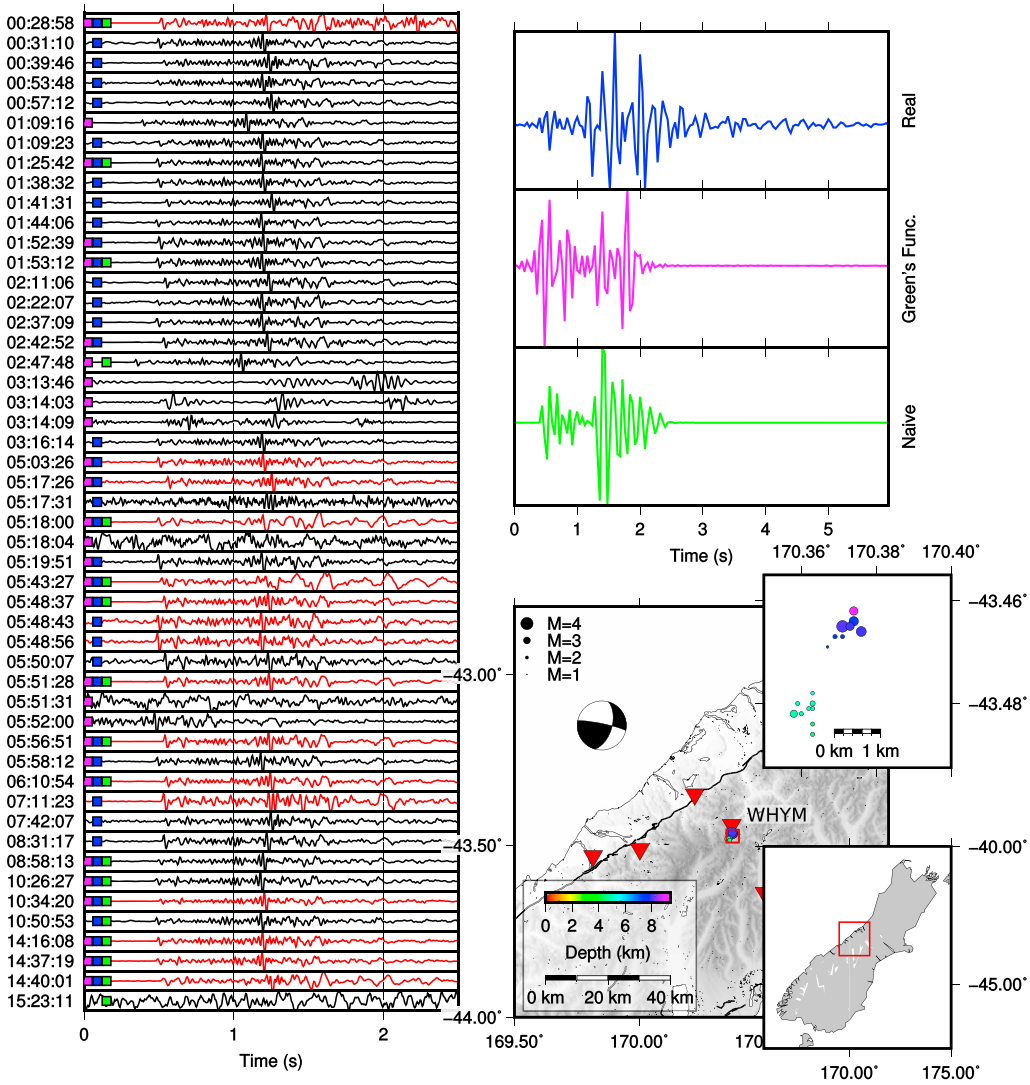

Figure 1. Detections made by three template sets for a swarm in the central Southern Alps. (left) Waveforms of detected events aligned on detection time: red waveforms are detections of an event in the initial catalog of Boese et al. (2014). Colored squares indicate which template made that detection (blue for real templates, pink for Green's function synthetic templates, and green for naïve synthetic templates). (top right) Template waveforms for the vertical channel of SAMBA station WHYM plotted with the same color coding as at left. (bottom right) Locations of template events (circles colored by depth and sized by magnitude) and the focal mechanism used for synthetic calculation. Inverted triangles mark seismic stations. The red box in the lower inset marks location of main map, with zoom top right.

for the templates derived from detections made by the Green's function and naïve synthetics, respectively. Using detections from real templates made 7,340 detections, but 3,577 appear to be duplicate detections (see supporting information Figure S18). The sta/lta detection yielded 682 detections for the same period.

3.3. Low-Frequency Earthquakes

New Zealand's Alpine Fault is known to display weak tremor (Wech et al., 2012) and LFEs (Baratin et al., 2018; Chamberlain et al., 2014). Low amplitudes and strong scattering preclude the use of LFE detection methods reliant on interstation coherence (such as beam forming (Frank & Shapiro, 2014) or cross station (Savard & Bostock, 2015) methods). Previous analysis of LFEs in the Southern Alps has relied on manual inspection of waveforms to first identify tremor, then find possible LFE waveforms within the tremor (Chamberlain et al., 2014). This is time-consuming and generates nonuniform catalogs that are likely to be biased. In this example, we demonstrate that LFE waveforms can be identified using synthetic templates appropriate to the source region.

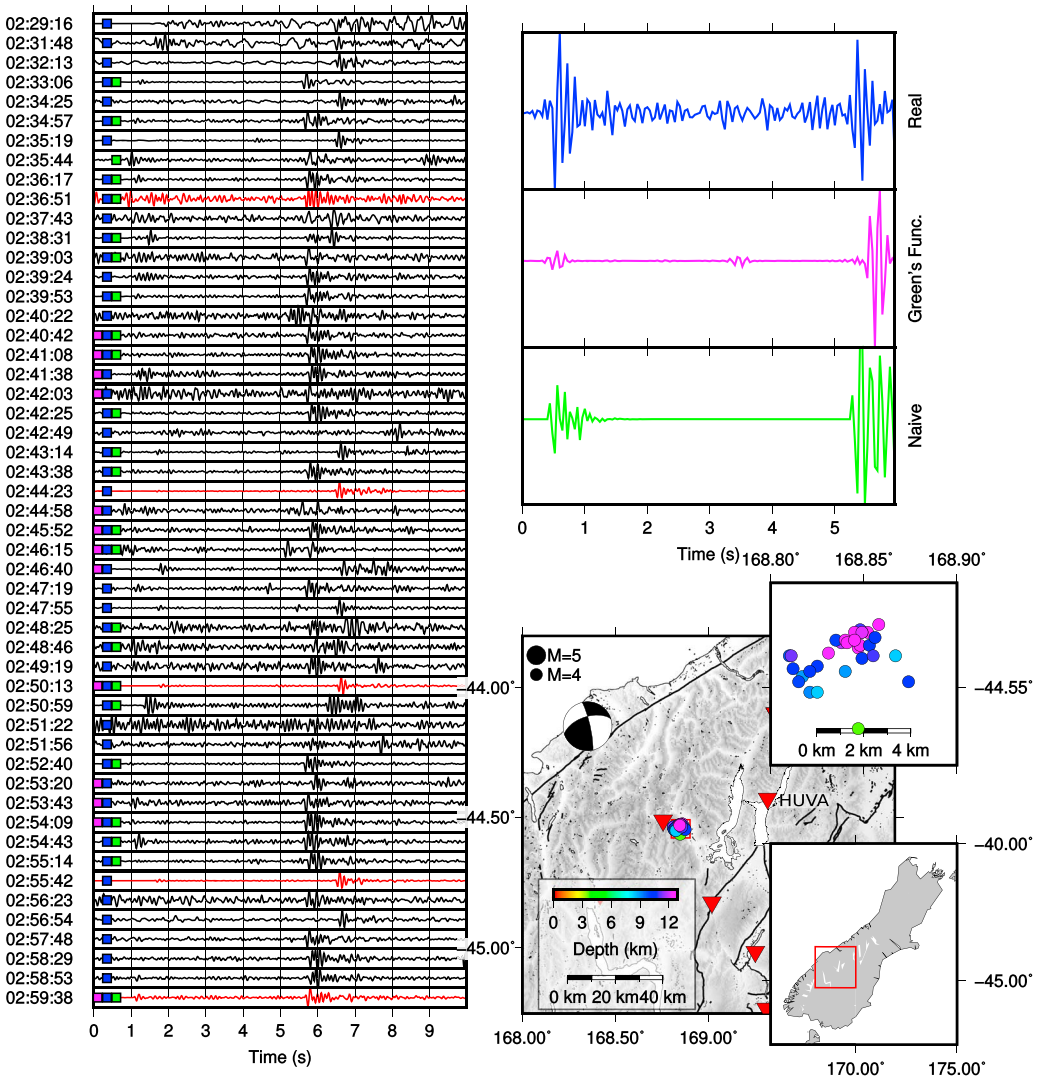

Figure 2. Detections made for 1 hr of the aftershock sequence of the *M*6.0 Wanaka earthquake. Note that for plotting purposes, only detections separated by >20 s are shown, which excludes 103 detections made by the real templates. Panels are as shown in Figure 1. Red waveforms are detections made within 20 s of an event listed in the GeoNet catalog for this region. Template waveforms for station HUVA, vertical channel are shown.

This case study extends the two previous examples by generating a set of synthetic templates for a grid of possible LFE source locations. Specifically, we generate grids of templates in a region 60 × 120 km horizontally and between 11 and 35-km depth, centered around −43.17°, 170.04° and rotated 57° clockwise from North to align with the local strike of the Alpine Fault. Templates are spaced every 2.5 km horizontally and 2 km vertically, generating a total of 15,925 source locations.

We generate naïve synthetic templates using predicted travel times for each source and station computed with *TauP* (Crotwell et al., 1999) and a composite 1-D velocity model using the South Island velocity model from Ristau (2008) embedded in the IASP91 global model (Kennett & Engdahl, 1991). To generate Green's functions, we use the velocity model of Ristau (2008) for South Island, and a representative focal mechanism from Baratin et al. (2018; 52/66/141, strike/dip/rake in degrees). We do not generate real templates in this example. Synthetic waveforms are generated for the seven stations closest to the template source. Using more distant stations resulted in fewer detections due to the low SNR of these events. Using fewer stations resulted in more false detections and detections associated with inconsistent source locations. All templates are resampled to 25 Hz, filtered between 1 and 5 Hz and cut to 15 s, beginning 0.5 s before the calculated *P* phase arrival. We

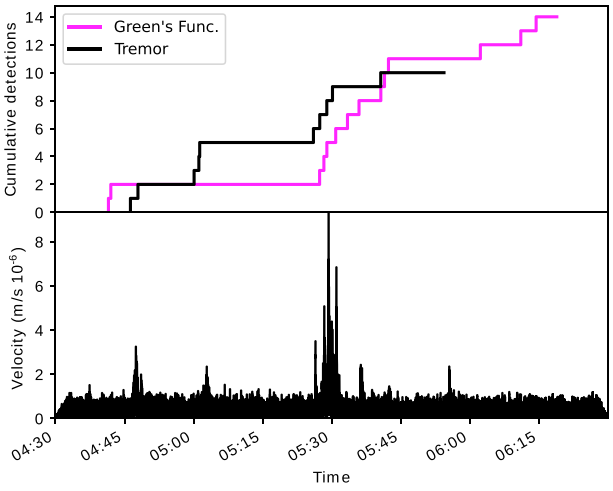

Figure 3. (top) Detections made by the Green's function synthetics during a period of known tremor (Wech et al., 2012) on 20 August 2010 UTC. Tremor times are bursts of at least 5 minutes of tremor (Wech et al., 2012) identified by manual inspection. (bottom) Envelope of data (filtered 1–10 Hz and resampled to 20 Hz) from station COVA, EH1 component.

use three channels at each station for every template. In this example the continuous data are corrected for instrument response, not the templates.

We correlate these template sets with 2 hr of data (20 August 2010, between 04:30 and 06:30 UTC), within which tremor was previously identified by Wech et al. (2012), and detect when the cross-correlation sum exceeds 10×MAD. Finally, we remove events within 20 s of another higher-correlating detection. Using *EQcorrscan* (Chamberlain et al., 2017) allows us to run the correlations in less than 15 min using 40 CPU threads. In other words, it would be possible using moderate computing resources to run large template sets faster than real time.

At this threshold level we make no detections using the naïve synthetics, but we make 14 detections using the Green's function synthetics (Figure 3). When we tested at lower thresholds we obtained more detections, including detections for the naïve synthetic set; however, the false-detection rate was higher than the true detection rate, resulting in a nearly Gaussian distribution of detections with time.

We also generate a grid of templates for the upper 11 km of the crust in the same way as the deeper grid (6,125 templates in total). This also yields no detections for the naïve synthetics; however, 37 detections are made by the Green's function synthetics. Some of the detection times between the deeper and shallower grids coincide, but the detections in the shallower grid are dominated by templates at the southern edge of the grid, furthest away from the stations used. These appear to be detections of LFEs incorrectly matched to shallow templates (see supporting information Figure S16). This highlights a weakness when applying this method far from the seismic network used: the depth constraint is lost (discussed further in section 4).

Detections cluster within bursts of previously documented tremor (Figure 3), they also have similar characteristics to manually identified LFEs in the central Southern Alps (e.g., dominant power in the 2–8 Hz band, emergent waveforms, weak *P* energy, and within previously determined tremor, see Figure S15). We suggest that this may provide a useful tool for detecting LFEs in this region, but care needs to be taken to ensure detections are correctly mapped to the best-fitting template. To do this we suggest detecting for long periods (multiple years spanning many tremor bursts), before correlating all detections with each other to regroup detections into families, then stacking these waveforms and using these real, stacked waveforms in a further matched-filter run. This will be conducted for the central Southern Alps LFEs in a future study.

We note that the naïve synthetics failed in this example. This is likely due to the emergent arrivals that are not well described by the naïve synthetics, and the lack of focal mechanism constraint. The best sta/lta detector we tried found eight detections, of which three are possible LFE detections and the others regional or distant earthquakes.

4. Sensitivity

To assess the sensitivity of detections to template locations, we generate a grid of 2,890 synthetic templates with source locations spaced every 2.5 km in all directions in a 40 × 40 × 22.5 km volume around one of the swarm events analyzed in section 3.1 (hereafter referred to as the target event). Only Green's function synthetics are considered in the following analysis, generated using the method described in section 3.1. We correlate all templates with the hour of data surrounding the time of the target event and detect when the cross-correlation sum exceeds 8×MAD. All detections within 2 s after the target event origin time are assumed to be the target event. The locations of each detecting template are plotted in Figure 4. Seventy-four Green's function synthetic templates detected the target event.

We use five stations with the target event occurring just inside the aperture of this subnetwork (Figure 4). Most detections arise from templates located outside of the subnetwork. This demonstrates that the specificity of a template to a source depends strongly on network geometry. The stripes of positive and negative correlation sums suggest that cycle skipping is occurring. Care must therefore be taken when interpreting detection locations from outside the network used. In particular this means that multiple events detected by the same

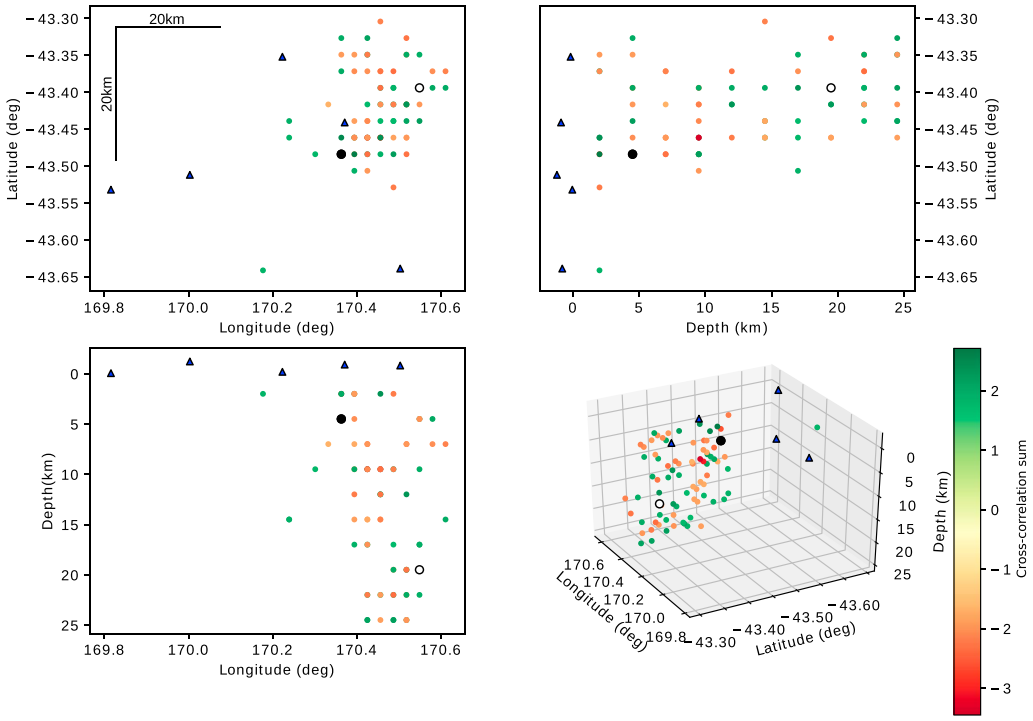

Figure 4. Geometry of location sensitivity test: Target event location (black circle), subnetwork used for detection (blue triangles), and locations of templates that detected the master event (circles colored by correlation sum). The template with the highest correlation sum is plotted as an open circle. Templates were created on a grid between −20 and 20 km in both North and East directions and between −20 km and 2.5 km depth, relative to the target event. Templates incorrectly associated with the master event generally fall outside the aperture of the subnetwork.

template should not simply be stacked together to form a high SNR waveform, a common technique when using real templates (e.g., Baratin et al., 2018; Chamberlain et al., 2014; Shelly & Hardebeck, 2010; Thurber et al., 2014), without further subclustering to ensure detected events are properly linked to other events.

We also test sensitivity to changes in focal mechanism, using the same swarm event and subnetwork. We generate a set of 13,824 Green's function synthetic templates (the naïve synthetics have no focal mechanism dependence) by varying the strike, dip, and rake of the target focal mechanism from −180 to 180° sampled every 15°. Of these 13,824 templates, 4,434 detected the target at the 8×MAD threshold used (see supporting information Figure S14).

The target event has an oblique strike-slip mechanism, but templates created using both thrust and normal mechanisms were also capable of detecting the event. Furthermore, templates with similarly striking and dipping nodal planes, but reversed rake (and therefore reversed polarities of incoming waves) were also capable of detecting the target event. We have allowed both negatively and positively correlated detections. However, not all of the detections from inverted mechanisms have a negative detection value, suggesting that cycle skipping may be occurring.

The sensitivity of a template to an event is clearly dependent on network geometry, and this likely holds when using real waveforms as templates as well. In both cases it would be prudent to compare detections from multiple templates to ensure that the detection is associated with the best-fitting location and focal mechanism. The apparent cycle skipping occurring when making detections with flipped polarities also suggests that cycle skipping may work to reduce similarity in detections made by a single template, and would effectively smear out arrivals if multiple detections were stacked together.

5. Discussion and Conclusions

In none of our examples did the synthetic templates outperform real templates in their ability to detect real earthquakes. However, in all cases shown, the synthetic templates were able to detect a variety of real waveforms, each of which could then be used as a template itself to create a dense catalog of seismicity. The

synthetic templates also outperformed standard energy detectors: more real detections were made than with previous energy detectors.

We specifically chose cases of clustered seismicity for our examples, where SNR is poor (due to either low amplitudes in the case of the LFEs or overlapping waveforms in the aftershock and swarm examples). We would not expect the synthetic templates to outperform standard energy detectors in cases where signal-to-noise is high.

We did not test for dependence on source size. Our simple synthetics do not capture the increased complexity of larger events, and we were unable to detect either the *M*6.0 Wanaka mainshock or the largest aftershock on that day (*M*4.1). We could model multiple sources and combine them to generate an extended source, but, in general, standard detection methods work well for such large events, so extending this study to large magnitudes seems of limited value.

We used simple 1-D velocity models in our examples, but other modeling codes that allow the use of 3-D models would allow more complex, and likely more realistic templates to be generated which may provide improved results. Previous work by Rodgers et al. (2006) included velocity model uncertainty to generate multiple possible waveforms for a fixed source and used the singular-value decomposition of these waveforms in a subspace routine to detect similar events. This is likely a useful extension to the work presented here, but involves further set-up time and further correlations, which will affect the final speed of the detection routine.

Single-channel correlations between synthetic and real waveforms are often low in our examples. However, when using a network of stations, these correlations sum to be significantly above the noise (meaning that the waveforms may not be coherent, but the correlations prove to be). Therefore, although we are doing a poor job of representing the complexity of the seismic source we are able to stack correlations coherently because we have a reasonable model for the travel time between source and receiver.

We foresee several possible applications of this method, in particular, to enhance detections early in aftershock sequences and during volcanic and nonvolcanic swarms, and to detect LFEs in regions with poor SNR and high scattering. This method is best used to generate a preliminary set of detections which could be used as real templates in a subsequent matched-filter run to generate a final catalog. Projects like *EQcorrscan* (Chamberlain et al., 2017) and *FastMatchedFilter* (Beaucé et al., 2017), which leverage parallel architectures, enable the large grids required to cover source regions to be constructed and used to detect earthquakes faster than real time.

Appendix A: Data and Resources

All codes and data for this project are available at https://bitbucket.org/calum-chamberlain/synthetic_method_examples/src/master/. This project leverages the *EQcorrscan* project for detection (Chamberlain et al., 2017). Codes also make use of *GMT* (*gmt-python*; Wessel & Smith, 1998), *ObsPy* (Beyreuther et al., 2010), *matplotlib*, *mpl-stereonet*, and *numpy*.

Acknowledgments
This project was supported by grants from the Marsden Fund of Royal Society of New Zealand (17-VUW-121) and the Earthquake Commission of New Zealand (18/753). We are grateful to William Frank for pointing out the *axitra* code and to Martha Savage for initial discussions. We acknowledge the New Zealand GeoNet project and its sponsors EQC, GNS Science, and LINZ, for providing data used in this study. We are grateful to David Shelly, Gavin Hayes and one anonymous reviewer for their constructive reviews which improved the manuscript.

References

Baratin, L.-M., Chamberlain, C. J., Townend, J., & Savage, M. K. (2018). Focal mechanisms and inter-event times of low-frequency earthquakes reveal quasi-continuous deformation and triggered slow slip on the deep Alpine Fault. *Earth and Planetary Science Letters*, *484*, 111–123. https://doi.org/10.1016/j.epsl.2017.12.021

Beaucé, E., Frank, W. B., & Romanenko, A. (2017). Fast matched filter (FMF): An efficient seismic matched-filter search for both CPU and GPU architectures. *Seismological Research Letters*, *89*(1), 165–172.

Beyreuther, M., Barsch, R., Krischer, L., Megies, T., Behr, Y., & Wassermann, J. (2010). ObsPy: A Python toolbox for seismology. *Seismological Research Letters*, *81*(3), 530–533. https://doi.org/10.1785/gssrl.81.3.530

Boese, C. M., Jacobs, K. M., Smith, E. G. C., Stern, T. A., & Townend, J. (2014). Background and delayed-triggered swarms in the central Southern Alps, South Island, New Zealand. *Geochemistry, Geophysics, Geosystems*, *15*, 945–964. https://doi.org/10.1002/2013GC005171

Boese, C. M., Townend, J., Smith, E., & Stern, T. (2012). Microseismicity and stress in the vicinity of the Alpine Fault, central Southern Alps, New Zealand. *Journal of Geophysical Research*, *117*, B02302. https://doi.org/10.1029/2011JB008460

Chamberlain, C. J., Hopp, C. J., Boese, C. M., Warren Smith, E., Chambers, D., Chu, S. X., & Townend, J. (2017). EQcorrscan: Repeating and near repeating earthquake detection and analysis in Python. *Seismological Research Letters*, *89*, 173–181. https://doi.org/10.1785/0220170151

Chamberlain, C. J., Shelly, D. R., Townend, J., & Stern, T. A. (2014). Low-frequency earthquakes reveal punctuated slow slip on the deep extent of the Alpine Fault, New Zealand. *Geochemistry, Geophysics, Geosystems*, *15*, 2984–2999. https://doi.org/10.1002/2014GC005436

Coutant, O. (1989). Program of numerical simulation AXITRA. Res. Rep. LGIT (in French), Universite Joseph Fourier, Grenoble.

Crotwell, H. P., Owens, T. J., & Ritsema, J. (1999). The TauP toolkit: Flexible seismic travel-time and ray-path utilities. *Seismological Research Letters*, *70*, 154–160.

Frank, W. B., & Shapiro, N. M. (2014). Automatic detection of low-frequency earthquakes (LFEs) based on a beamformed network response. *Geophysical Journal International*, *197*(2), 1215–1223. https://doi.org/10.1093/gji/ggu058

Frank, W. B., Shapiro, N. M., Kostoglodov, V., Husker, A. L., Campillo, M., Payero, J. S., & Prieto, G. A. (2013). Low-frequency earthquakes in the Mexican sweet spot. *Geophysical Research Letters*, *40*, 2661–2666. https://doi.org/10.1002/grl.50561

Gerstenberger, M. C., Wiemer, S., Jones, L. M., & Reasenberg, P. A. (2005). Real-time forecasts of tomorrow's earthquakes in California. *Nature*, *435*(7040), 328–331.

Gibbons, S. J., & Ringdal, F. (2006). The detection of low magnitude seismic events using array-based waveform correlation. *Geophysical Journal International*, *165*(1), 149–166. https://doi.org/10.1111/j.1365-246X.2006.02865.x

Hainzl, S. (2016). Rate-dependent incompleteness of earthquake catalogs. *Seismological Research Letters*, *87*(2A), 337–344.

Kato, A., & Obara, K. (2014). Step-like migration of early aftershocks following the 2007 M_w 6.7 Noto-Hanto earthquake, Japan. *Geophysical Research Letters*, *41*, 3864–3869. https://doi.org/10.1002/2014GL060427

Kato, A., Obara, K., Igarashi, T., Tsuruoka, H., Nakagawa, S., & Hirata, N. (2012). Propagation of slow slip leading up to the 2011 M_w 9.0 Tohoku-Oki earthquake. *Science*, *335*(6069), 705–708. https://doi.org/10.1126/science.1215141

Kennett, B., & Engdahl, E. (1991). Traveltimes for global earthquake location and phase identification. *Geophysical Journal International*, *105*(2), 429–465.

Ohta, K., & Ide, S. (2017). Resolving the detailed spatiotemporal slip evolution of deep tremor in Western Japan. *Journal of Geophysical Research: Solid Earth*, *122*, 10,009–10,036. https://doi.org/10.1002/2017JB014494

Peng, Z., & Zhao, P. (2009). Migration of early aftershocks following the 2004 Parkfield earthquake. *Nature Geoscience*, *2*(12), 877–881. https://doi.org/10.1038/ngeo697

Petersen, T., Gledhill, K., Chadwick, M., Gale, N. H., & Ristau, J. (2011). The New Zealand national seismograph network. *Seismological Research Letters*, *82*(1), 9–20. https://doi.org/10.1785/gssrl.82.1.9

Ristau, J. (2008). Implementation of routine regional moment tensor analysis in New Zealand. *Seismological Research Letters*, *79*(3), 400–415. https://doi.org/10.1785/gssrl.79.3.400

Rodgers, A., Harris, D., & Pasyanos, M. (2006). A model-based signal processing approach to seismic monitoring. In *Proceedings of 28th Seismic Research Review: Ground-Based Nuclear Explosion Monitoring Technologies: Orlando, FL* (pp. 455–464).

Savard, G., & Bostock, M. G. (2015). Detection and location of low frequency earthquakes using cross station correlation. *Bulletin of the Seismological Society of America*, *105*(4), 2128. https://doi.org/10.1785/0120140301

Shelly, D. R., Beroza, G. C., & Ide, S. (2007). Non-volcanic tremor and low-frequency earthquake swarms. *Nature*, *446*, 305–307. https://doi.org/10.1038/nature05666

Shelly, D. R., Ellsworth, W. L., Ryberg, T., Haberland, C., Fuis, G. S., Murphy, J., & Bu, R. (2009). Precise location of San Andreas Fault tremors near Cholame, California using seismometer clusters: Slip on the deep extension of the fault? *Geophysical Research Letters*, *36*, L01303. https://doi.org/10.1029/2008GL036367

Shelly, D. R., & Hardebeck, J. L. (2010). Precise tremor source locations and amplitude variations along the lower crustal central San Andreas Fault. *Geophysical Research Letters*, *37*, L14301. https://doi.org/10.1029/2010GL043672

Shelly, D. R., Hill, D. P., Massin, F., Farrell, J., & Smith, R. B. (2013). A fluid-driven earthquake swarm on the margin of the Yellowstone caldera. *Journal of Geophysical Research: Solid Earth*, *118*, 4872–4886. https://doi.org/10.1002/jgrb.50362

Shelly, D. R., Moran, S. C., & Thelen, W. A. (2013). Evidence for fluid-triggered slip in the 2009 Mount Rainier, Washington earthquake swarm. *Geophysical Research Letters*, *40*, 1–7. https://doi.org/10.1002/grl.50354

Slinkard, M. E., Carr, D. B., & Young, C. J. (2013). Applying waveform correlation to three aftershock sequences. *Bulletin of the Seismological Society of America*, *103*(2A), 675–693. https://doi.org/10.1785/0120120058

Thurber, C. H., Zeng, X., Thomas, A. M., & Audet, P. (2014). Phase-weighted stacking applied to low-frequency earthquakes. *Bulletin of the Seismological Society of America*, *104*(5), 2567–2572.

Warren-Smith, E., Chamberlain, C. J., Lamb, S., & Townend, J. (2017). High-precision analysis of an aftershock sequence using matched filter detection: The 4 May 2015 ML 6 Wanaka earthquake, Southern Alps, New Zealand. *Seismological Research Letters*, *88*(4), 1065–1077. https://doi.org/10.1785/0220170016

Warren-Smith, E., Fry, B., Kaneko, Y., & Chamberlain, C. J. (2018). Foreshocks and delayed triggering of the 2016 MW7.1 Te Araroa earthquake and dynamic reinvigoration of its aftershock sequence by the MW7.8 Kaikura earthquake, New Zealand. *Earth and Planetary Science Letters*, *482*, 265–276. https://doi.org/10.1016/J.EPSL.2017.11.020

Warren-Smith, E., Lamb, S., Stern, T. A., & Smith, E. (2017). Microseismicity in Southern South Island, New Zealand: Implications for the mechanism of crustal deformation adjacent to a major continental transform. *Journal of Geophysical Research: Solid Earth*, *122*, 9208–9227. https://doi.org/10.1002/2017JB014732

Wech, A. G., Boese, C. M., Stern, T. A., & Townend, J. (2012). Tectonic tremor and deep slow slip on the Alpine Fault. *Geophysical Research Letters*, *39*, L10303. https://doi.org/10.1029/2012GL051751

Wessel, P., & Smith, W. H. (1998). New, improved version of Generic Mapping Tools released. *Eos, Transactions American Geophysical Union*, *79*(47), 579–579.